Contents lists available at ScienceDirect

Quaternary Science Reviews

journal homepage: www.elsevier.com/locate/quascirev

Online Supplement 1 for

Asynchronous glaciations in arid continental climates

Jigjidsurengiin Batbaatar[a, *], Alan R. Gillespie[a, **], David Fink[b], Ari Matmon[c], Toshiyuki Fujioka[b]

[a] *Quaternary Research Center, University of Washington, Seattle, WA 98195-1310, USA.*
[b] *Australian Nuclear Science and Technology Organisation, PMB1, Menai, 2234, Australia.*
[c] *The Institute of Earth Sciences, Hebrew University of Jerusalem, Givat Ram, Jerusalem 91904, Israel*

* Corresponding author.

** Corresponding author.

Email addresses: bataa@uw.edu (J. Batbaatar); arg3@uw.edu (A.R. Gillespie)

https://doi.org/10.1016/j.quascirev.2017.12.001

Online Supplement Fig. 1. Field photos of some of the sampled boulders. a, b, c, Samples from the Gichginii range (GN-JB- 001, 003, 005). d, e, f, Samples from the southwestern slope of the Sutai range (SUT-JB- 02D, 04A, and SUT-IM-01B). g, h, i, Samples from the Ih Bogd range (IB-JB- 003E, 003B, 001). j, k, l, Samples from the Bogd river valley in Otgontenger (OT-AG- 1, 2, 3). m, n, o, Samples from the Bumbat valley in the Hangai ranges (HN-JB-01A, 02B, 03A). The hammer, hand-held GPS unit, and a notebook are for scale.

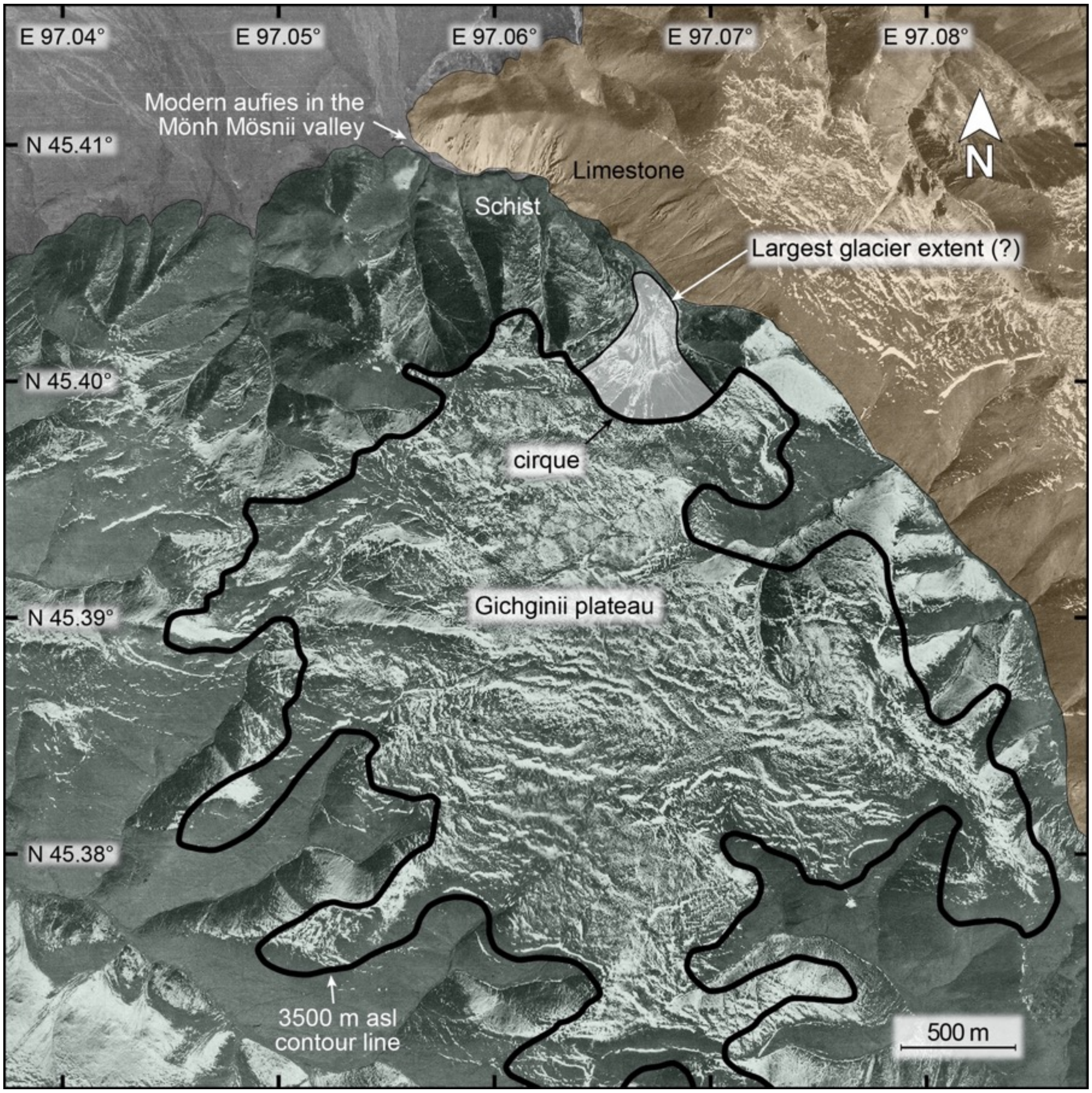

Online Supplement Fig. 2. Gichginii plateau and maximum glacial extent in the Mönh Mösnii valley. The extent of the largest glacier in the Mönh Mösnii valley is based on the outermost extent of the G2 moraine. A contour line at 3500 m asl roughly delineates the extent of the plateau. The bedrocks in the upper right part of the photo (tan) is limestone, and the bedrocks in the lower left part (gray-green) is schist. Aerial photo was taken in winter of 1957 (National Archives of Mongolia).

Online Supplement Fig. 3. The tan-weathering gray limestone boulders on the G1 ridge in the Mönh Mösnii cirque. The white veins (left center) are calcite. The photographer was facing northwest.

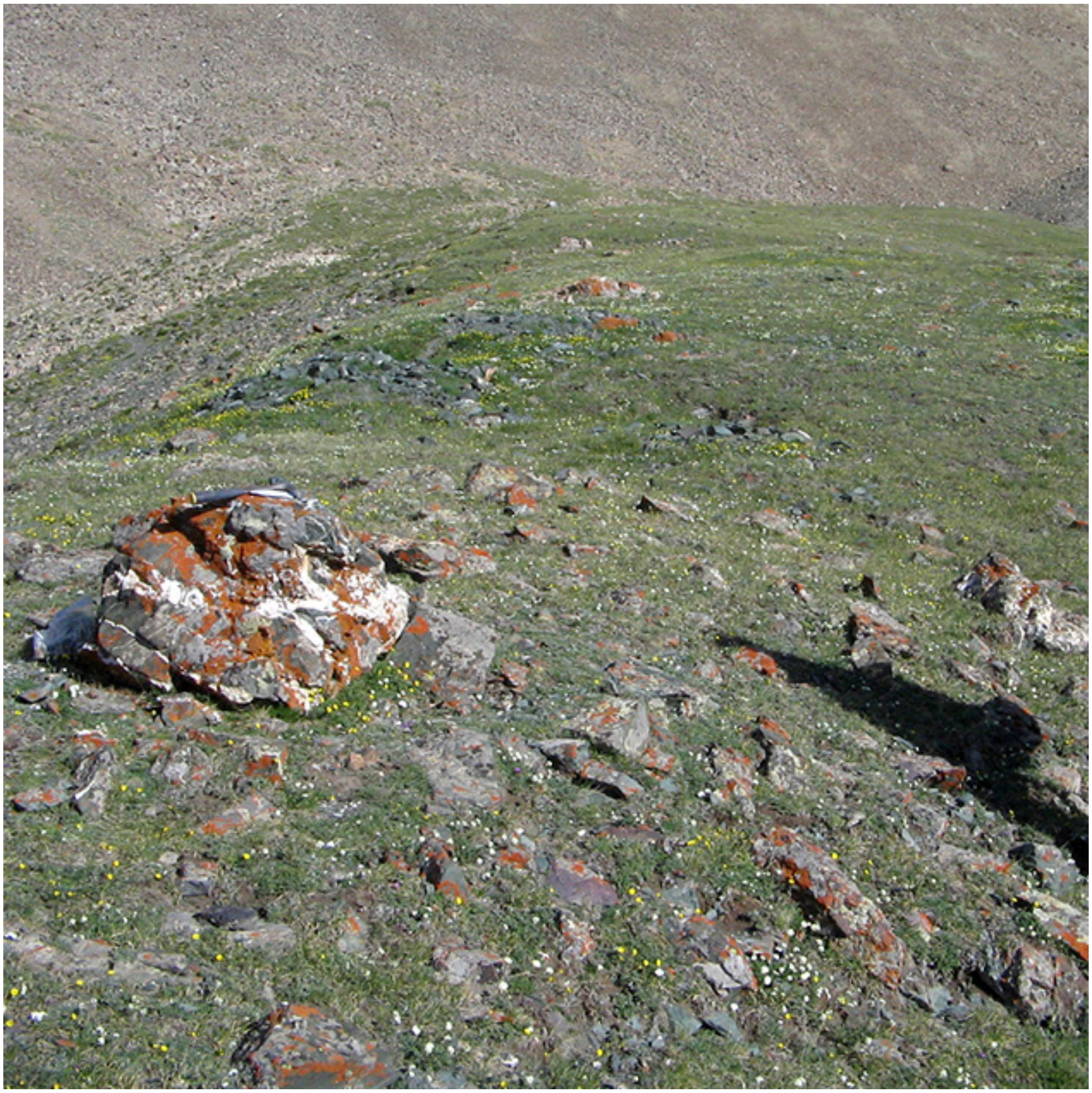

Online Supplement Fig. 4. Surface of the upper part of the G2 moraine. The quartz vein from the singular boulder (GN-JB-005) was sampled for ^{10}Be analysis. The fractures in the boulder suggests heavy erosion, but the lack of broken pieces surrounding the boulder suggests the boulder could have been a rock fallen on supraglacial till. Note the hammer on top of the boulder for scale. The photographer was facing southeast.

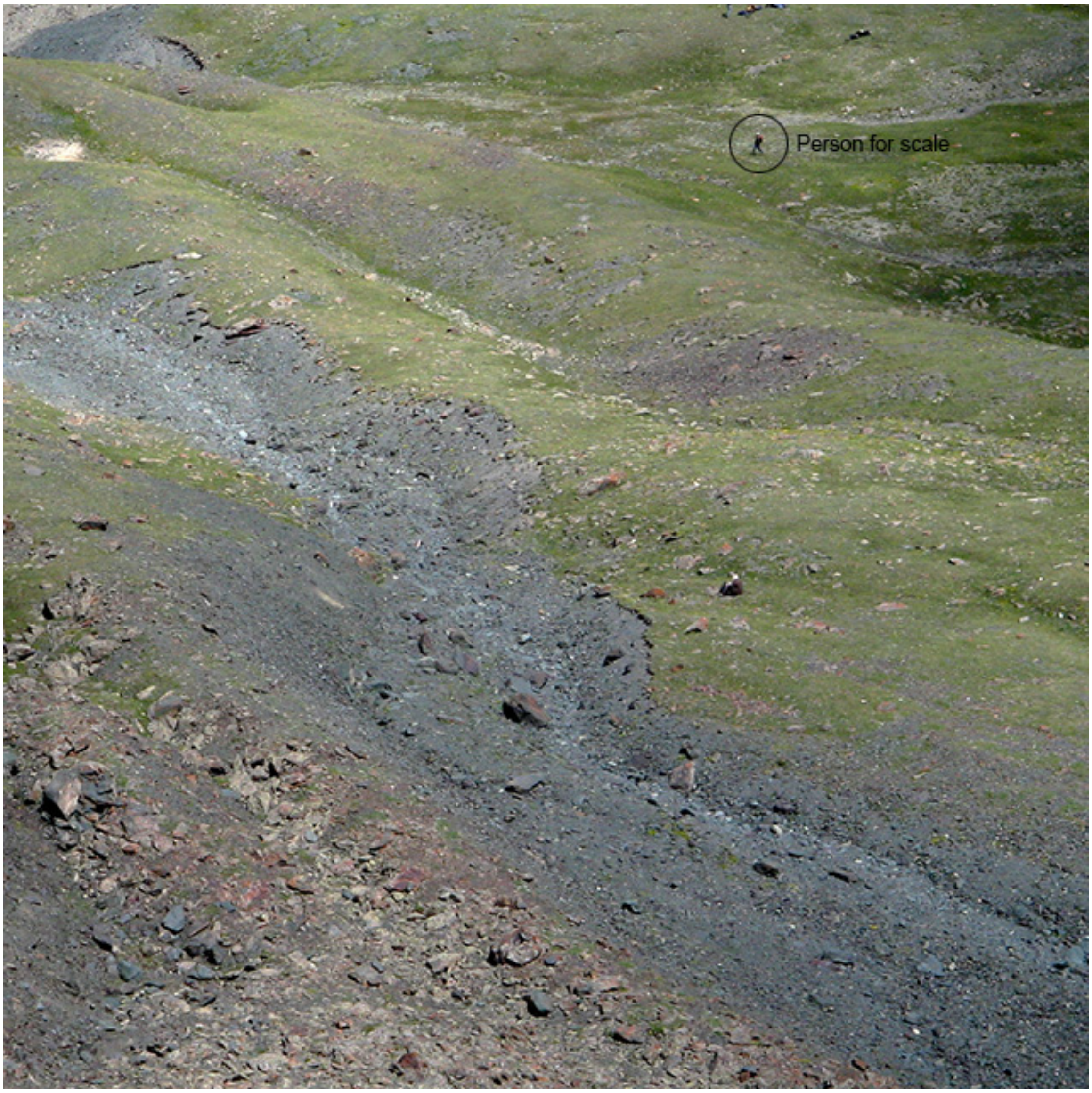

Online Supplement Fig. 5. Surface features of the upper part of the G3 moraine. The photo was taken from the headwall slope in the south, above the moraine G5. Note people in the photo for scale (top right). G2 moraine is at the top, partly out of the frame. The photographer was facing northeast.

Online Supplement Fig. 6. Surface features of the lower part of the moraine G4. Beyond the green moraine ridge (G3, top center) the slope of the valley increases. The photographer was facing north.

Outlier identification of ^{10}Be ages

Our work covered a broad, complex area and the number of dated samples per moraine was smaller than desired in order to characterize a population with a well-determined arithmetic mean and standard deviation. In studies such as this, identification of outliers is important, and commonly problematic. Key assumptions used in cosmic-ray exposure dating of glacial boulders—no inheritance, preservation of sample orientation and constant ^{10}Be production—predict a normal distribution of ages with low standard deviation roughly equal to analytical uncertainty. Large standard deviation of a population scatter is in question if dating for glacial boulders assumes no transportation of boulders after the initial deposition, and field context is helpful to sort through the distribution of ages. We used series of analyses to identify outliers in the following order: 1) calculate the mean, μ_{group}, and standard deviation, σ_{group}, for n ages grouped according to landform; 2) calculate the reduced chi-squared value, $R\chi^2$, for n ages to test if the scatter in the group cannot be explained by analytical uncertainty alone; 3) for each sample i, calculate the normalized deviation, δ_i, from the mean calculated excluding the age of the tested sample, x_i. Samples for which δ_i>2 were rejected as outliers; 4) test whether in sequence of moraines the ^{10}Be ages were consistent with the relative ages of the moraines inferred geomorphically; 5) recalculate the $R\chi^2$ excluding the outliers; 6) evaluate the identified outliers using Chauvenet's (1960) and Peirce's (Ross, 2003) criterion to confirm that the surviving group samples contained no outliers. After excluding the outliers, we averaged the sample ages for a given landform and compounded standard deviation of the "reduced" group with the "internal" sample measurement uncertainties with the systematic uncertainties in the production and decay rates of ^{10}Be ("external" uncertainties). We report this 1σ total uncertainty as the duration of glacier advances or standstills for the given landform. Below we describe each of the analysis in detail.

Reduced chi-squared test…It is defined as the chi-square per degree of freedom as below:

$$R\chi^2 = \frac{\chi^2}{n-1}$$

where $R\chi^2$ is the reduced chi-square, n is sample number in the group. The χ^2 is calculated as:

$$\chi^2 = \sum_{i=n}^{n} \frac{\left(x_i - \mu_{group}\right)}{\sigma_i}$$

where x_i is the age of sample i, μ_{group} is the mean of the grouped ages, and σ_i is the internal uncertainty of sample i.

Normalized deviation from the mean…For each sample, the normalized deviation from the mean, δ_i, was calculated as below:

$$\delta_i = \frac{|x_i - \mu_{n-i}|}{\sqrt{(\sigma_{n-i}{}^2 + \sigma_i{}^2)}}$$

where μ_{n-i} is the mean of the grouped ages excluding the tested sample age x_i, σ_{n-i} is the standard deviation of the grouped ages excluding the tested sample age x_i. The sample was identified as outlier if the $\delta_i > 2$.

Chauvenet's criterion… In Chauvenet's test it is assumed that the population is normally distributed and characterized by a mean and standard deviation (1σ), and the normalized probability of a data point in the distribution is calculated. If the product of the probability of data point and the number of samples falls below 0.5, the data point is rejected as an outlier. The normal variance, z, is calculated as below:

$$z = \frac{|x_i - \mu_{group}|}{\sigma_{group}}$$

where σ_{group} is the standard deviation of the grouped ages. Next, normal density function was calculated using the NORMDIST(x_i, μ_{group}, σ_{group},TRUE) function of Microsoft Excel, in which the TRUE denotes that the NORMDIST function is calculating the cumulative distribution function from negative infinity to x_i. If the $z > 0.5$ the tail of the normal distribution is calculated as $2(1-z)$, or if $z < 0.5$ the tail of the normal distribution is calculated as $2z$. Finally, these values were multiplied by the sample number to calculate the Chauvenet's criterion value. The sample age is rejected if the Chauvenet's criterion value < 0.5.

Peirce's criterion… We used Ross' (2003) tabulated tables of Peirce R values to confirm the identified outliers. In Peirce's test the maximum allowable deviation of the group is calculated by multiplying a tabulated value corresponding to the number of samples and the standard deviation of the group, σ_{group}, and then compared to the actual deviation of a sample age from the mean, $|x_i - \mu_{group}|$. The data point is rejected if the deviation of the sample age from the mean is greater than the maximum allowable deviation, which is dependent on the sample number and standard deviation of the age group, and is unique to the grouped ages. We provide the formulae used in the calculations in Online Supplement 2 (Excel spreadsheet).

We also used the modified Kolmogorov-Smirnov test formulated by Lilliefors (1967). The Lilliefors formulation is commonly used to test whether the population is from a normal distribution when the mean and variance are unknown. We used the built-in function “lillietest” in Matlab. According to the Matlab documentation, the Lilliefors test statistic is defined as:

$$D^* = \left(x_i - \mu_{group}\right)\left|\hat{F}(x) - G(x)\right|$$

where $\hat{F}(x)$ is the empirical cumulative density function, and $G(x)$ is the hypothesized cumulative density function characterized by μ_{group} and σ_{group}.

In all age groups the Lilliefors test returned 0 logical answer at its default 5% significance level, which means that either 1) the population was normally distributed; or 2) the sample number was too low to reject the hypothesis that it wasn’t.

Identification of outliers within a population of cosmogenic exposure ages depends largely on the AMS measurement quality of the dataset, the number of samples in the population expected to be coeval and the inherent variability of geologic processes associated with the preservation of the landform. Statistically, increasing the number of samples can define a population better, which can lead to a clearer selection of outliers from a well-defined population. However, if the exposure variability due to geologic processes is sufficiently great, simply doing more analyses will not improve the precision or accuracy of the age of the moraine. For small sample sets, the consistency between the exposure ages and the sample positions with the sequence of moraines may provide the only criterion with which to identify an outlier.

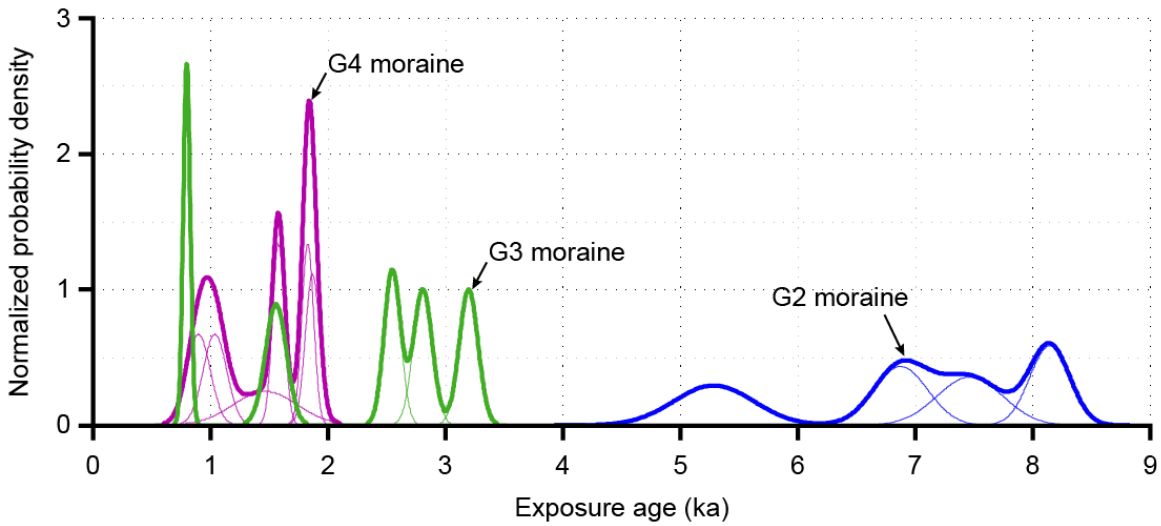

Online Supplement Fig. 7. Normalized probability curves created using G. Balco's Matlab code (http://depts.washington.edu/cosmolab/pubs/gb_pubs/camelplot.m) for the ^{10}Be ages for the moraines in Gichginii range. The thin lines are probability curves for individual samples (internal uncertainties only), and the thick lines are sum of the individual probability curves. Three of the four ^{10}Be ages from the G2 moraine (blue lines) overlap with each other within 2σ internal uncertainty, and constrain the exposure age for this moraine to ~8–7 ka (1σ age range after rejecting outliers). The remaining ^{10}Be age, 5.3 ± 0.3 ka, does not overlap with the older cluster and is regarded as an outlier. Three ^{10}Be ages from the G3 moraine (green lines) overlap within 2σ internal uncertainty around 3.5–2.2 ka (2σ age range of the mean after rejecting outliers). The remaining two ^{10}Be ages do not overlap at all, and are regarded as outliers. Four of the six ^{10}Be ages from the G4 moraine (purple lines) formed a mode around 2–1.5 ka. The remaining two ^{10}Be ages at ~0.9 ka overlaps with the youngest age from the older cluster, mainly due to its high (18%) 1σ uncertainty. Nevertheless, the younger cluster is only 600 yr apart from the older cluster, suggesting that the G4 moraine was formed ~2–0.8 ka (2σ age range of the mean after rejecting outliers). Probability curves for all ^{10}Be ages, including three outliers, show the oldest advance of the Gichginii glaciation at ~9–6 ka, with subsequent glacier re-advances or standstills at ~3.5–2.2 ka and ~2.1–0.8 ka.

Online Supplement Table 1

^{10}Be data used for exposure-age calculation

Site	Group	Sample	Location	Altitude (m asl)	Thick-ness (cm)	Production rate (atoms g^{-1} yr^{-1})		Shielding factor	Quartz[c] (g)	Be carrier (mg)	$^{10}Be/^{9}Be$[d,e] ($\times 10^{-15}$)	^{10}Be concentration[e,f] (10^3 atoms g^{-1} SiO_2)	Age[g,h] (ka ± 1σ)
						Spallation[a]	Muons[b]						
Gichginii range (Gobi-Altai)	G2	GN-AG-10B	45.4038/97.0704	3289	1	44.90	0.51	0.99	9.0144	0.2678	157.13 ± 5.06	311.9 ± 10.3	6.9 ± 0.4
		GN-AG-11	45.4038/97.0704	3289	2	44.53	0.51	0.99	10.4866	0.2681	214.35 ± 3.99	366.2 ± 7.6	8.1 ± 0.5
		GN-JB-004	45.4023/97.0702	3327	2	45.54	0.52	0.99	13.8520	0.2121	237.72 ± 10.39	243.2 ± 15.4	5.3 ± 0.4
		GN-JB-005	45.4039/97.0703	3283	2	44.37	0.51	0.99	11.5540	0.2149	269.29 ± 6.69	334.7 ± 12.7	7.5 ± 0.5
	G3	GN-AG-07	45.4014/97.0701	3340	2	45.89	0.52	0.99	9.7160	0.2685	39.26 ± 2.27	72.5 ± 4.2	1.6 ± 0.1
		GN-AG-08	45.4014/97.0701	3340	2	45.89	0.52	0.99	9.2480	0.2682	76.58 ± 1.74	148.4 ± 3.5	3.2 ± 0.2
		GN-AG-04	45.4015/97.0697	3361	2	46.46	0.52	0.99	10.0974	0.2520	22.42 ± 0.74	37.4 ± 1.2	0.8 ± 0.1
		GN-AG-05	45.4015/97.0697	3361	5	45.33	0.51	0.99	10.0976	0.2520	77.31 ± 2.13	128.9 ± 3.6	2.8 ± 0.2
		GN-AG-06	45.4015/97.0697	3361	1	46.84	0.52	0.99	10.0581	0.2516	72.35 ± 1.86	120.9 ± 3.2	2.6 ± 0.2
	G4	GN-JB-001	45.4022/97.0686	3330	2	45.62	0.52	0.99	16.5650	0.2262	45.48 ± 3.44	41.5 ± 4.5	0.9 ± 0.1
		GN-JB-002	45.4024/97.0686	3330	2	45.62	0.52	0.99	10.7350	0.2135	36.03 ± 2.45	47.9 ± 4.7	1.0 ± 0.1
		GN-JB-003	45.4025/97.0689	3336	2	45.78	0.52	0.99	7.4880	0.2135	35.80 ± 4.58	68.2 ± 12.4	1.5 ± 0.3
		GN-AG-01	45.4013/97.0697	3338	1	46.21	0.52	0.99	9.7453	0.2693	46.25 ± 1.28	85.4 ± 2.4	1.8 ± 0.1
		GN-AG-02	45.4013/97.0697	3338	2	45.83	0.52	0.99	11.5492	0.2678	55.77 ± 1.65	86.4 ± 2.6	1.9 ± 0.1
		GN-AG-03	45.4013/97.0697	3338	2	45.83	0.52	0.99	9.4141	0.2686	38.30 ± 1.12	73.0 ± 2.2	1.6 ± 0.1
Sutai range (Gobi-Altai)	NE1	DHC-98-12	46.6418/93.5710	3160	2	41.09	0.49	0.96	39.3700	0.2530	709.99 ± 17.30	304.9 ± 11.4	7.3 ± 0.5
	NE2–4	DHC-98-13	46.6418/93.5659	3240	2	44.03	0.50	0.98	39.8300	0.2520	2744.67 ± 53.94	1160.4 ± 36.2	26.2 ± 1.7
		DHC-98-10	46.6403/93.5648	3270	2	43.92	0.51	0.96	39.9400	0.2500	2421.74 ± 45.69	1012.9 ± 30.6	22.9 ± 1.5
		DHC-98-11	46.6404/93.5661	3250	5	42.78	0.50	0.97	31.7100	0.2540	2003.22 ± 61.99	1072.2 ± 49.3	24.9 ± 1.8
		DHC-98-15	46.6398/93.5652	3265	2	43.78	0.51	0.96	39.1700	0.3030	577.37 ± 13.13	298.4 ± 10.5	6.7 ± 0.4
	Pass between ice caps 1 & 2	MOT98-CS-11a	46.6323/93.5688	3620	1	55.44	0.57	0.98	39.9300	0.2520	5907.10 ± 88.38	2491.1 ± 63.4	45.0 ± 2.8
		MOT98-CS-11b	46.6323/93.5688	3620	1	55.44	0.57	0.98	10.5700	0.2510	465.15 ± 14.23	738.1 ± 33.6	13.2 ± 0.9
		MOT98-CS-12	46.6315/93.5688	3630	2	55.29	0.56	0.98	26.5000	0.2530	2156.31 ± 92.61	1375.6 ± 85.8	24.8 ± 2.1
	Ice cap 3 margin	SUT-JB-04A	46.6052/93.6192	3934	4	66.20	0.61	1	19.7590	0.2460	206.70 ± 6.50	1400.9 ± 26.9	21.3 ± 1.2
		SUT-JB-04B	46.6044/93.6194	3926	3	65.91	0.61	1	19.6910	0.2641	1023.60 ± 16.40	2737.0 ± 64.9	41.6 ± 2.5
	Bedrock & erratic	MOT98-CS-22	46.6012/93.5490	3105	2.5	40.86	0.48	0.99	39.2900	0.2510	2127.87 ± 49.57	908.4 ± 32.6	22.1 ± 1.5
		MOT98-CS-23	46.6012/93.5490	3105	2.5	40.86	0.48	0.99	39.7200	0.2520	6918.88 ± 158.50	2933.2 ± 103.7	72.4 ± 4.8
	SW remnant	MOT98-CS-14	46.6094/93.5522	3180	2.5	42.68	0.49	0.99	9.0000	0.2520	814.53 ± 28.02	1524.0 ± 77.2	35.6 ± 2.7
	SW 2	MOT98-CS-25	46.6101/93.5475	3189	1	43.44	0.50	0.99	40.0500	0.2510	624.02 ± 15.38	261.3 ± 9.8	6.0 ± 0.4
		SUT-JB-02A	46.6126/93.5495	3238	1	44.76	0.51	0.99	20.4500	0.2669	796.90 ± 11.90	695.0 ± 17.7	15.4 ± 0.9
		SUT-JB-02B	46.6132/93.5503	3241	4	43.75	0.50	0.99	18.9490	0.2724	909.40 ± 17.50	873.6 ± 26.8	19.8 ± 1.3
		SUT-JB-02C	46.6132/93.5503	3241	2	44.47	0.50	0.99	20.1050	0.2711	692.40 ± 10.80	623.9 ± 16.3	13.9 ± 0.9
		SUT-JB-02D	46.6147/93.5520	3267	4	44.44	0.50	0.99	20.6780	0.2850	755.50 ± 14.50	695.8 ± 21.3	15.5 ± 1.0
Ih Bogd range (Gobi-Altai)	IB6	IB-JB-003E	44.9563/100.2668	3385	3	46.84	0.53	0.98	7.8410	0.2503	364.34 ± 18.53	777.1 ± 57.0	16.7 ± 1.5
		IB-JB-003A	44.9563/100.2668	3390	3	46.94	0.53	0.98	5.9830	0.4383	69.25 ± 3.24	339.0 ± 22.9	7.3 ± 0.6
		IB-JB-003B	44.9563/100.2668	3390	3	46.94	0.53	0.98	7.3950	0.2489	274.24 ± 25.56	616.7 ± 81.8	13.2 ± 1.9
		IB-JB-003C	44.9563/100.2668	3390	5	46.94	0.53	0.98	6.4350	0.2475	254.66 ± 8.98	654.4 ± 33.9	14.3 ± 1.1
		IB-JB-003D	44.9563/100.2668	3390	5	46.94	0.53	0.98	7.5470	0.2503	288.64 ± 13.29	639.6 ± 42.6	13.9 ± 1.2
	IB5	IB-JB-002	44.9567/100.2672	3402	3	46.14	0.52	0.97	26.643	0.3963	627.71 ± 22.11	623.9 ± 32.3	13.4 ± 1.0
	IB7	IB-JB-001	44.9578/100.2675	3425	5	47.53	0.53	0.97	2.3380	0.2446	95.71 ± 3.82	669.2 ± 38.9	14.4 ± 1.2

Online Supplement Table 1 (continued)

^{10}Be data used for exposure age calculation

Site	Group	Sample	Location	Altitude (m asl)	Thick-ness (cm)	Production rate (atoms g^{-1} yr^{-1})		Shielding factor	Quartz[c] (g)	Be carrier (mg)	^{10}Be/^{9}Be[d,e] ($\times 10^{-15}$)	^{10}Be concentration[e,f] (10^{3} atoms g^{-1} SiO_2)	Age[g,h] (ka ± 1σ)
						Spallation[a]	Muons[b]						
Otgontenger peak (Hangai)	BO1	OT-AG-1	47.6833/97.2067	2075	5	20.74	0.35	0.99	6.7680	0.2121	226.90 ± 8.44	475.2 ± 25.9	22.7 ± 1.8
		OT-AG-2	47.6833/97.2067	2075	5	20.74	0.35	0.99	7.8800	0.2135	234.02 ± 10.86	423.7 ± 28.4	20.2 ± 1.8
		OT-AG-3	47.6833/97.2067	2075	5	20.74	0.35	0.99	7.4390	0.2149	255.90 ± 9.65	494.0 ± 27.3	23.6 ± 1.9
	BI2	DHC-98-5	47.5755/97.6677	2580	3	30.20	0.42	1	39.1400	0.2520	2209.51 ± 41.75	950.6 ± 28.7	31.3 ± 2.0
		DHC-98-7	47.5755/97.6677	2580	3	30.20	0.42	1	8.3200	0.2520	1228.23 ± 23.44	2485.9 ± 75.7	82.9 ± 5.3
		DHC-98-8	47.5755/97.6677	2580	3	30.20	0.42	1	32.9000	0.2530	1767.67 ± 33.29	908.3 ± 27.4	29.9 ± 1.9
	BI8	MOT98-CS-02	47.5978/97.6497	2725	2.5	33.47	0.44	0.98	40.7200	0.2530	1292.31 ± 31.4	536.5 ± 19.9	16.2 ± 1.1
	BI9	DHC-98-3	47.6035/97.6403	2725	2.5	32.72	0.43	0.98	40.0700	0.2550	1164.20 ± 27.15	495.1 ± 17.8	15.0 ± 1.0
		MOT98-CS-04	47.6035/97.6405	2725	2.5	32.72	0.43	0.98	38.6600	0.2520	1253.91 ± 23.7	546.2 ± 16.5	16.5 ± 1.0
		MOT98-CS-05	47.6035/97.6405	2725	2.5	32.72	0.43	0.98	31.3700	0.3030	849.20 ± 16.25	548.1 ± 16.7	16.6 ± 1.1
Bumbat valley (Hangai)	BU1	HN-JB-01B	47.4355/100.3471	2128	2	22.24	0.36	1	7.5740	0.2530	1023.60 ± 16.40	2284.8 ± 61.0	103.7 ± 6.5
		HN-JB-01C	47.4355/100.3471	2128	3	22.06	0.36	1	6.6310	0.2697	436.55 ± 6.90	1186.5 ± 31.4	53.6 ± 3.3
		HN-JB-01A	47.4357/100.3468	2130	3	22.09	0.36	1	6.7270	0.2446	206.70 ± 6.50	502.2 ± 23.4	22.5 ± 1.6
	BU2	HN-JB-02A	47.4158/100.3573	2172	3	22.52	0.37	0.99	4.0770	0.2836	108.53 ± 3.04	504.5 ± 21.2	22.2 ± 1.5
		HN-JB-02B	47.4164/100.3559	2173	4	22.36	0.37	0.99	2.0590	0.2585	106.04 ± 2.93	889.6 ± 37.0	39.5 ± 2.8
		HN-JB-02C	47.4164/100.3559	2173	3	22.54	0.37	0.99	5.5590	0.2836	211.83 ± 4.85	722.1 ± 25.5	31.8 ± 2.1
		HN-JB-03A	47.4180/100.3525	2177	5	22.46	0.37	1	6.8460	0.2738	309.30 ± 7.50	826.6 ± 30.7	36.5 ± 2.5
		HN-JB-03B	47.4180/100.3525	2177	4	22.65	0.37	1	11.5840	0.2780	452.40 ± 17.30	725.5 ± 40.6	31.8 ± 2.5
		HN-JB-03C	47.4180/100.3525	2177	5	22.46	0.37	1	6.5930	0.2794	397.00 ± 9.20	1124.2 ± 40.1	49.9 ± 3.3
Non-glacial deposits at Sutai (Gobi-Altai)		MOT98-CS-20	46.6068/93.5628	3205	3	43.16	0.50	0.99	39.0000	0.2520	95.47 ± 6.61	41.2 ± 4.1	0.9 ± 0.1
		MOT98-CS-21	46.6068/93.5628	3205	3	43.16	0.50	0.99	39.7800	0.2520	164.00 ± 7.18	69.4 ± 4.4	1.6 ± 0.1
		MOT98-CS-08	46.6160/93.5639	3273	2.5	45.16	0.51	0.99	39.3600	0.2520	1263.39 ± 29.04	540.5 ± 19.2	11.9 ± 0.8
		DHC-98-17	46.6168/93.5645	3290	3	44.97	0.51	0.98	34.6500	0.3050	313.60 ± 7.33	184.5 ± 6.6	4.1 ± 0.3
		DHC-98-18	46.6168/93.5645	3290	1	45.72	0.51	0.98	34.3200	0.3030	1426.30 ± 27.03	841.4 ± 25.5	18.3 ± 1.2
		MOT98-CS-19	46.6168/93.5645	3290	3	44.97	0.51	0.98	39.4900	0.2530	98.67 ± 9.12	42.2 ± 5.6	0.9 ± 0.1
		SUT-IM-01A	46.6177/93.5656	3310	4	44.22	0.51	0.96	15.4490	0.2655	101.47 ± 3.01	116.5 ± 4.3	2.6 ± 0.2
		SUT-IM-01B	46.6177/93.5656	3310	3	44.58	0.51	0.96	14.2310	0.2724	101.65 ± 2.92	130.0 ± 4.7	2.9 ± 0.2
		SUT-IM-01C	46.6177/93.5656	3310	2	44.95	0.51	0.96	16.2570	0.2627	116.98 ± 3.83	126.3 ± 5.0	2.8 ± 0.2

[a] Constant (time-invariant) ^{10}Be production rate value of 3.99 ± 0.22 atoms g^{-1} yr^{-1} (Heyman, 2014) scaled by method of Lal (1991) and Stone (2000).

[b] Constant (time-invariant) local production rate based on Heisinger et al. (2002a, 2002b).

[c] Density of 2.65 g cm^{-3} was used based on the quartz vein and granitic composition of the surface samples.

[d] AMS isotope ratios measured at LLNL were normalized to ^{10}Be/Be standards prepared by Nishiizumi et al. (2007) with a nominal value of ^{10}Be/Be = 2.85 × 10^{-12}. Samples measured at ANSTO (see Fink & Smith 2007) were normalized to the NIST 4325-SRM with a ^{10}Be/Be value of 27.9 × 10^{-12} or 07KN-5-2 with a ^{10}Be/Be value of 8.56 × 10^{-12}. All three standard reference materials are internally consistent (see Nishiizumi et al., 2007).

[e] Uncertainties are reported at the 1σ confidence level.

[f] Propagated uncertainties include uncertainty in the blank, carrier concentration (1%), and counting statistics.

[g] Propagated 1σ "external" uncertainty in the model age includes "internal" uncertainties introduced in (f) in addition to a 5.5 % uncertainty in the production rate of ^{10}Be and a 1% uncertainty in the ^{10}Be decay constant. All ^{10}Be concentrations were converted to ages using a ^{10}Be half-life of 1.389 × 10^{6} yr (Chmeleff et al., 2010) using CRONUS-Earth calculator version 2.2 (Balco et al., 2008) to calculate the ages. The ^{10}Be standard is called 07KNSTD in CRONUS-Earth.

[h] We assumed zero erosion of the rock and no burial history. An erosion rate of 3 mm yr^{-1} would increase an age of 30 ka by ~10% (Batbaatar and Gillespie, 2016).

Online Supplement Table 2

Temperature and relative humidity measurements for the Sutai range. We used an EL-USB-2 sensor from Lascar Electronics to measure T_a and humidity above the surface of ice cap #3. The sensors were placed at 4000 m asl and 1.8 m above the ice surface. Weather data for 2200 m asl are from Tonhil town, 40 km southeast of Sutai (NOAA, 2016). The average of our measured near-surface lapse rate (8 °C km^{-1}) was greater than the annually measured lapse rate in the Italian Alps (~6.0 °C km^{-1}: Rolland 2002) and the modeled maximum lapse rates in the Cascade Mountains, Washington State, USA (6.5–7.5 °C km^{-1}: Minder et al., 2010). The lower lapse rate used in the surface-energy model would increase T_a overall, which lengthened the melting season by 1–2 months and decreased the snowfall by 15–20% in the studied sites. However, the increased T_a in winter and spring makes the ice surface warmer, leading to increased sublimation (e.g., Cuffey and Paterson, 2010).

Date	Relative Humidity (%)		Mean Daily T_a (°C)		Lapse rate (°C km^{-1})
	2200 m asl	4000 m asl	2200 m asl	4000 m asl	
5/24/2013	31	76	10.1	−6.7	9.4
5/25/2013	41	81	8.0	−8.2	9.0
5/26/2013	44	77	4.9	−11.0	8.8
5/27/2013	47	83	1.6	−13.3	8.3
5/28/2013	23	45	7.9	−6.5	8.0
5/29/2013	29	56	11.3	−3.2	8.0
5/30/2013	39	74	8.1	−5.5	7.5
5/31/2013	32	48	7.0	−5.6	7.0
6/1/2013	15	43	11.7	−4.7	9.1
6/2/2013	24	56	12.9	−1.7	8.1
6/3/2013	37	85	14.2	−2.3	9.2
6/4/2013	37	70	14.3	−0.7	8.4
6/5/2013	39	74	13.7	−1.0	8.2
6/6/2013	42	62	10.5	−2.3	7.1
6/7/2013	30	70	9.8	−5.1	8.3
6/8/2013	42	81	6.2	−9.3	8.6
6/9/2013	24	47	10.4	−3.2	7.5
6/10/2013	17	34	15.2	1.7	7.5
6/11/2013	19	51	17.2	0.8	9.1
6/12/2013	32	57	11.2	−3.2	8.0
6/13/2013	51	80	8.8	−4.5	7.4
6/14/2013	66	89	7.8	−5.4	7.3
6/15/2013	48	74	9.7	−4.4	7.8
6/16/2013	44	77	10.7	−3.3	7.8
6/17/2013	31	61	14.5	−1.1	8.7
6/18/2013	26	62	16.0	1.1	8.3
6/19/2013	37	78	16.2	1.0	8.5
6/20/2013	82	100	9.6	−1.2	6.0
6/21/2013	73	100	11.1	−1.2	6.8
6/22/2013	79	100	11.7	−0.7	6.9
Average	**39**	**70**	**10.7**	**−3.7**	**8.0**

Online Supplement Table 3

Summary of modern climate at the study sites scaled with a lapse rate of 7.9 °C km^{-1} (average of measured summer T_a in Supplement Table 2). The table below includes monthly mean air temperature (T_a, °C: Kalnay et al., 1996), total precipitation (P, mm: Schneider et al., 2016), and zonal mean solar insolation (S, W m^{-2}). The lower part of the table shows the seasonal and annual mean T_a where winter is December–February, spring is March–May, summer is June–August, and autumn is September–November. Aridity index and corresponding environmental classification (Zomer et al., 2008) are included. Precipitation as snow or rain was not available.

	Gichginii 3380 m asl		Sutai 3870 m asl		Ih Bogd 3470 m asl		Otgontenger 3800 m asl		Bumbat 3100 m asl		45°N
	T_a	P	T_a	P	T_a	P	T_a	P	T_a	P	S
January	−28.7	1	−33.9	1	−30.2	2	−34.1	1	−28.9	2	149
February	−24.8	1	−30.6	1	−26.3	1	−30.6	2	−25.6	2	225
March	−17.4	2	−24.1	2	−18.7	5	−23.6	4	−18.6	6	313
April	−8.2	2	−15.6	4	−9.2	5	−14.8	5	−9.4	10	403
May	−0.1	3	−8.5	12	−1.1	10	−7.1	11	−1.5	26	464
June	5.8	6	−2.6	24	4.7	14	−1.3	25	4.3	51	485
July	7.8	17	0	31	6.8	33	0.9	48	6.4	78	461
August	5.5	13	−1.7	24	4.4	23	−1.2	34	4.2	64	398
September	−0.9	6	−7.8	10	−2.0	12	−7.4	16	−2.0	20	309
October	−10.1	2	−16.6	4	−11.1	4	−16.1	6	−10.6	11	218
November	−20.3	1	−26.4	1	−21.5	2	−26.2	3	−20.8	5	146
December	−27.3	1	−32.5	1	−28.7	2	−32.6	2	−27.3	3	121
Winter	−26.9	2	−32.3	3	−28.4	6	−32.4	5	−27.3	7	165
Spring	−8.6	7	−16.1	18	−9.7	19	−15.2	20	−9.8	42	393
Summer	6.4	37	−1.4	79	5.3	69	−0.5	107	5.0	194	448
Autumn	−10.4	9	−16.9	16	−11.5	18	−16.6	25	−11.1	36	225
Annual	−9.9	55	−16.7	115	−11.1	112	−16.2	158	−10.8	279	308
Aridity index		0.2		0.5		0.4		0.6		0.6	
Classification		arid		semi-arid		semi-arid		dry sub-humid		dry sub-humid	

Online Supplement Table 4

Regional changes in climate parameters during global LGM and early Holocene compared to modern values. The table shows the anomalies in annual and summer mean air temperature (T_a), annual precipitation (P), and zonal mean solar insolation (S) at 45°N for global LGM (Owen et al., 1998; Bintanja and van de Wal, 2008; Braconnot 2007; Annan and Hargreaves, 2013) and for early Holocene (Herzschuh, 2006; Miehe et al., 2007; Bintanja and van de Wal, 2008; Jin et al., 2012) compared to modern means. Summer is the mean for June–August, and winter is the mean for December–February.

	Units	22 ka (global LGM)	8 ka (early Holocene)
Summer ΔT_a	°C	−8	3
Annual ΔT_a	°C	−16	−2
Annual ΔP	mm yr^{-1}	× 0.75	× 2
Summer ΔS	W m^{-2}	−5	26
Winter ΔS	W m^{-2}	2	−10

References in Online Supplement 1

Annan, J.D., Hargreaves, J.C., 2013. A new global reconstruction of temperature changes at the Last Glacial Maximum. Clim. Past 9, 367–376.

Balco, G., Stone, J.O., Lifton, N.A., Dunai, T.J., 2008. A complete and easily accessible means of calculating surface exposure ages or erosion rates from ^{10}Be and ^{26}Al measurements. Quat. Geochronol. 3, 174–195.

Balco, G. 2011. What is a camel diagram anyway? The bleeding edge of cosmogenic-nuclide geochemistry. https://cosmognosis.wordpress.com/2011/07/25/what-is-a-camel-diagram-anyway/

Batbaatar, J., Gillespie, A.R., 2016. Outburst floods of the Maly Yenisei. Part II – new age constraints from Darhad basin. Int. Geol. Rev. 58, 1753–1779.

Bintanja, R., van de Wal, R.S.W., 2008. North American ice-sheet dynamics and the onset of 100,000-year glacial cycles. Nature 454, 869–872.

Braconnot, P., Otto-Bliesner, B., Harrison, S., Joussaume, S., Peterchmitt, J.Y., Abe-Ouchi, A., Crucifix, M., Driesschaert, E., Fichefet, Th., Hewitt, C.D., Kageyama, M., Kitoh, A., Laîné, A., Loutre, M.F., Marti, O., Merkel, U., Ramstein, G., Valdes, P., Weber, S.L., Yu, Y., Zhao, Y., 2007. Results of PMIP2 coupled simulations of the Mid-Holocene and Last Glacial Maximum – Part 1: experiments and large-scale features. Clim. Past 3, 261–277.

Chauvenet, W., 1960. Reprint of 1891, fifth ed.. A Manual of Spherical and Practical Astronomy V. II. 1863, pp. 473–566, Dover, N.Y.

Chmeleff, J., von Blanckenburg, F., Kossert, K., Jakob, D., 2010. Determination of the ^{10}Be half-life by multicollector ICP-MS and liquid scintillation counting. Nucl. Instr. Meth. Phys. Res. B. 268, 192–199.

Cuffey, K.M., Paterson, W.S.B., 2010. The Physics of Glaciers, fourth ed. Elsevier, Amsterdam.

Fink, D., Smith, A., 2007. An inter-comparison of ^{10}Be and ^{26}Al AMS reference standards and the ^{10}Be half-life. Nucl. Instr. Meth. Phys. Res. B. 259, 600–609.

Heisinger, B., Lal, D., Jull, A.J.T., Kubik, P., Ivy-Ochs, S., Neumaier, S., Knie, K., Lazarev, V., Nolte, E., 2002a. Production of selected cosmogenic radionuclides by muons: 1. Fast muons. Earth Planet. Sci. Lett. 200, 345–355.

Heisinger, B., Lal, D., Jull, A.J.T., Kubik, P., Ivy-Ochs, S., Neumaier, S., Knie, K., Lazarev, V., Nolte, E., 2002b. Production of selected cosmogenic radionuclides by muons: 2. Capture of negative muons. Earth Planet. Sci. Lett. 200, 357–369.

Herzschuh, U., 2006. Palaeo-moisture evolution in monsoonal Central Asia during the last 50,000 years. Quaternary Sci. Rev. 25, 163–178.

Heyman, J., 2014. Paleoglaciation of the Tibetan Plateau and surrounding mountains based on exposure ages and ELA depression estimates. Quat. Sci. Rev. 91, 30–41.

Jin, L., Chen, F., Morrill, C., Otto-Bliesner, B.L., Rosenbloom, N., 2012. Causes of early Holocene desertification in arid central Asia. Clim. Dyn. 38, 1577–1591.

Kalnay, E., Kanamitsu, M., Kistler, R., Collins, W., Deaven, D., Derber, J., Gandin, L., Saha, S., White, G., Woollen, J., Zhu, Y., Chelliah, M., Ebisuzaki, W., Higgins, W., Janowiak, J., Mo, K.C., Ropelewski, C., Wang, J., Leetma, A., Reynolds, R., Jenne, R., 1995. The NCEP/NCAR 40-year re-analysis project. Bull. Amer. Meteor. Soc. 77, 437–471.

Kargel, J.S., Leonard, G.J., Bishop, M.P., Kääb, A., Raup, B.H. (Eds.), 2014. Global Land Ice Measurements from Space, Springer Praxis Books, Springer, Berlin.

Lal, D., 1991. Cosmic ray labeling of erosion surfaces: In situ nuclide production rates and erosion models. Earth Planet. Sci. Lett. 104, 424–439.

Lilliefors, H.W., 1967. On the Kolmogorov-Smirnov test for normality with mean and variance unknown. J. Am. Stat. Assoc. 62, 399–402.

Miehe, G., Schültz, F., Miehe, S., Opgenoorth, L., Cermak, J., Samiya, R., Jäger, E.J., Wesche, K., 2007. Mountain forest islands and Holocene environmental changes in Central Asia: A case study from the southern Gobi Altay, Mongolia. Palaeogeogr. Palaeoclimatol. Palaeoecol. 250, 150–166.

Minder, J.R., Mote, P.W., Lundquist, J.D., 2010. Surface temperature lapse rates over complex terrain: Lessons from the Cascade Mountains. J. Geophys. Res. 115, D14122, doi:10.1029/2009JD013493.

National Oceanic and Atmospheric Administration (NOAA), 2016. Integrated Surface Database (ISD), Station Tonhil USAF ID 442660. Accessed from http://www.ncdc.noaa.gov/isd in October 2016.

Nishiizumi, K., Imamura, M., Caffee, M., Southon, J., Finkel, R., McAnich, J., 2007. Absolute calibration of ^{10}Be AMS standards. Nucl. Instr. Meth. Phys. Res. B. 258, 403–413.

Ohmura, A., Kasser, P., Funk, M., 1992. Climate at the equilibrium line of glaciers. J. Glaciol. 38, 397–411.

Owen, L.A., Richards, B., Rhodes, E.J., Cunningham, W.D., Windley, B.F., Badamgarov, J., Dorjnamjaa, D., 1998. Relic permafrost structures in the Gobi of Mongolia: age and significance. J. Quaternary Sci. 13, 539–547.

Porter, S.C., 2001. Snowline depression in the tropics during the Last Glaciation. Quat. Sci. Rev. 20, 1067–1091.

Rolland, C., 2002. Spatial and seasonal variations of air temperature lapse rates in Alpine region. J. Clim. 16, 1032–1046.

Ross, S.M., 2003. Peirce's criterion for the elimination of suspect experimental data. J. Eng. Technol., 20, 38–41.

Schneider, U., Becker, A., Finger, P., Meyer-Christoffer, A., Rudolf, B., Ziese, M., 2016. GPCC Full Data Reanalysis Version 7.0: Monthly Land-Surface Precipitation from Rain Gauges built on GTS based and Historic Data. Research Data Archive at the National Center for Atmospheric Research, Computational and Information Systems Laboratory. https://doi.org/10.5065/D6000072. Accessed January 2016.

Stone, J.O., 2000. Air pressure and cosmogenic isotope production. J. Geophys. Res. 105, 23753–23759.

Zomer, R.J., Trabucco, A., Bossio, D.A., Verchot, L.V., 2008. Climate change mitigation: A spatial analysis of global land suitability for clean development mechanism afforestation and reforestation. Agric. Ecosyst. Environ. 126, 67–80.